ACS Medicinal Chemistry Letters

pubs.acs.org/acsmedchemlett

Note

Fragment-Based Discovery of Novel MUS81 Inhibitors

Gavin W. Collie,* Ulf Börjesson, Yunhua Chen, Zhiqiang Dong, Paolo Di Fruscia, Andrea Gohlke, Anna Hoyle, Thomas A. Hunt, Mehul H. Jesani, Haiou Luo, Jakub Luptak, Alexander G. Milbradt, Priyanka Narasimhan, Martin Packer, Saleha Patel, Jingchuan Qiao, R. Ian Storer, Christopher J. Stubbs, Jonathan Tart, Caroline Truman, Anderson T. Wang, Matthew G. Wheeler, and Jon Winter-Holt

Cite This: *ACS Med. Chem. Lett.* 2024, 15, 1151−1158

Read Online

ABSTRACT: MUS81 is a structure-selective endonuclease that cleaves various branched DNA structures arising from natural physiological processes such as homologous recombination and mitosis. Due to this, MUS81 is able to relieve replication stress, and its function has been reported to be critical to the survival of many cancers, particularly those with dysfunctional DNA-repair machinery. There is therefore interest in MUS81 as a cancer drug target, yet there are currently few small molecule inhibitors of this enzyme reported, and no liganded crystal structures are available to guide hit optimization. Here we report the fragment-based discovery of novel small molecule MUS81 inhibitors with sub-μM biochemical activity. These inhibitors were used to develop a novel crystal system, providing the first structural insight into the inhibition of MUS81 with small molecules.

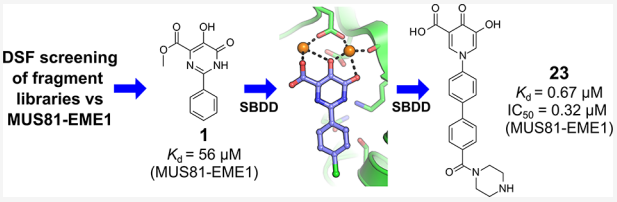

KEYWORDS: *Endonuclease, small molecule inhibitor, cancer drug discovery, crystallography, fragments*

MUS81 is a structure-selective endonuclease that, when in complex with EME1, cleaves various branched DNA structures (such as Holliday Junctions) arising from natural physiological processes including homologous recombination and genetic recombination.[1−4] As homologous recombination is one of the major pathways by which cells repair DNA damage, MUS81 contributes to the maintenance of genome stability. As such, there is evidence in support of its function as a tumor suppressor.[5−8] Paradoxically, however, several recent studies have now implicated MUS81 activity in playing a role in the progression of several cancers, such as serous ovarian cancer and leukemia.[9,10] Additionally, inhibition of MUS81 activity has been shown to sensitize certain ovarian cancers to chemotherapeutic agents such as cisplatin, as well as to poly-ADP ribose polymerase inhibitors.[9,11−13] There is thus interest in MUS81 as a potential cancer drug target, yet few small molecule inhibitors of this endonuclease have been reported.[14] Here, we report the fragment-based discovery of novel small molecule inhibitors of MUS81-EME1. Hit optimization resulted in compounds with sub-μM biochemical activity and favorable physicochemical and *in vitro* ADMET properties. We also report a series of crystal structures of MUS81-EME1-inhibitor complexes, providing the first structural insight into small molecule inhibition of the MUS81 endonuclease. Together, these results provide a structural and chemical basis for the further exploration of MUS81 as a potential cancer drug target.

A fragment-based hit finding approach was pursued as a means to find small molecule inhibitors of MUS81. Inspection of the few crystal structures available for human MUS81[15,16] strongly suggested the catalytic site of the enzyme to be the only site on the protein viable for targeting with small molecules. The catalytic site of MUS81 is dominated by a cluster of catalytic acidic residues expected to bind two Mg^{2+} ions.[15,16] Due to this, we designed a small library composed of around 360 fragment-sized molecules (MW < 350 Da) bearing chemical motifs known, or expected, to bind one or two metal (e.g., Mg^{2+}) ions. We then screened this library, along with a more standard fragment library composed of around 800 chemically diverse compounds, against a truncated form of the human MUS81-EME1 heterodimer[17] using differential scanning fluorimetry (DSF) (for full details, see the Supporting Information). All fragments were screened against the enzyme at a final concentration of 1 mM, in the presence of either 10 mM $MgCl_2$ or 10 mM EDTA, or in the absence of additive.[18] The metal-binding library yielded a primary hit rate of around 2.5%, with the chemically diverse library yielding a primary hit rate of only 0.9%. Fragments identified as potential hits by DSF were then analyzed by surface plasmon resonance (SPR) to confirm binding and determine K_d values for MUS81-EME1 (full experimental details can be found in the Supporting

Received: October 13, 2023
Revised: May 12, 2024
Accepted: May 16, 2024
Published: June 7, 2024

https://doi.org/10.1021/acsmedchemlett.3c00453
ACS Med. Chem. Lett. 2024, 15, 1151−1158

Information). From these experiments, around 10 fragments from the metal-binding library were confirmed as true binders of MUS81-EME1, with measured K_d values in the double-digit μM range or weaker, with compound **1** standing out as the most promising hit, with a K_d of 56 μM (Figures 1 and S1). No hits from the diverse library were validated when tested by SPR and were not followed up further.

Before attempting to characterize compound **1** structurally or biochemically, we first sought to increase its potency through limited SAR exploration by SPR to assess affinities for MUS81-EME1. Fairly confident that the pyrimidinone motif of **1** would be chelating to the two Mg^{2+} ions expected to be present in the active site of MUS81, we attempted to increase the potency of compound **1** by (1) optimizing Mg^{2+} binding, and (2) exploring substitutions and replacements of the phenyl ring. Replacement of the methyl ester group of the pyrimidinone with primary, secondary or tertiary amides (compounds **2**, **3**, and **4**) all led to a loss or significant reduction in affinity (Table 1). Replacement of the methyl ester with an acidic group (**5**), however, led to a significant increase in potency (~20-fold), and gave us further confidence that this series was indeed binding to the Mg^{2+} ions of the catalytic site of MUS81.

We next explored the phenyl group of this series, focusing on the acid **5** (Table 1). Replacement of the phenyl ring with a methyl (**6**) led to a ~20-fold drop in potency. While not surprising, the reduction in affinity was perhaps not as great as expected, and again reinforced Mg-chelation as the likely mode by which these compounds were binding to MUS81. Replacement of the phenyl ring with the equivalent saturated group (**7**) resulted in no change in affinity, and we thus pursued the phenyl group for further exploration due to the increased synthetic tractability of the aromatic system over the unsaturated system. Chloro substitution at the *ortho* or *meta* positions of the phenyl ring of **5** (**8** and **9**) slightly reduced binding affinity, while similar substitution at the *para* position (**10**) led to a noticeable (~2-fold), if modest, increase in affinity. Substitution at the *para* position of the phenyl ring

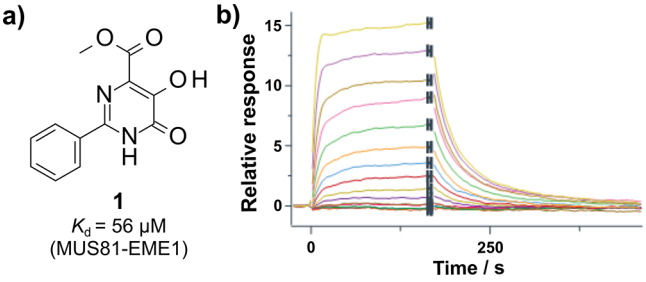

Figure 1. (a) Chemical structure of compound **1**. (b) Surface plasmon resonance sensorgrams of **1** for binding to MUS81-EME1.

with bromide (**11**) had a similar effect (~2-fold increase in affinity for MUS81), as did replacement of the phenyl ring with a β-naphthyl group (**12**).

With compounds in-hand displaying single-digit μM affinity for MUS81-EME1, we decided to use these compounds as tools to develop a biochemical assay to allow us to assess the ability of these compounds to inhibit the enzymatic function of MUS81. A fluorescence quenching-based assay using branched DNA as a substrate was thus developed (see the Supporting Information for full details) with assessment of compounds

Table 1. Activity and Efficiency Metrics of Pyrimidinone Derivatives against MUS81

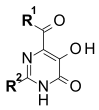

Cmpd	R^1	R^2	IC_{50} (μM)[a] SPR K_d (μM)[a]	LE[b] LLE[c]
1	OMe		>100 56 (0.85)	-
2	NH_2		>100 >100	-
3	NHMe		>100 74 (0.70)	-
4	$N(Me)_2$		>100 >100	-
5	OH		3.9 ± 0.3 2.3 (0.60)	0.44 6.4
6	OH	Me	>100 44 (0.62)	-
7	OH		2.8 ± 0.3 2.2 (0.56)	0.45 6.5
8	OH		3.8 ± 0.6 4.0 (0.61)	0.41 6.4
9	OH		5.6 ± 0.7 4.8 (0.66)	0.40 6.3
10	OH		2.1 ± 0.2 1.1 (0.52)	0.43 6.7
11	OH		2.0 ± 1.5 1.0 (0.61)	0.43 6.6
12	OH		1.5 ± 0.1 1.3 (0.72)	0.38 6.9
13	OH		4.5 ± 0.3 4.3 (0.34)	0.32 6.3
14	OH	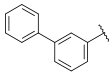	2.0 ± 0.3 1.8 (0.74)	0.34 7.4
15	OH	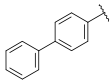	2.4 ± 0.2 0.72 (0.83)	0.33 5.9
16	OH	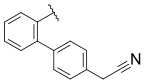	2.8 ± 0.3 0.54 (0.88)	0.29 4.6
17	OH	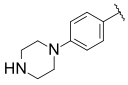	1.2 ± 0.3 2.1 (0.68)	0.35 6.9

[a]IC_{50} and K_d values are the geometric mean ± SEM (for IC_{50} values) or geometric standard deviation (for K_d values) of at least three determinations. [b]LE (kcal/mol/HA): 1.37 × pIC_{50}/HAC (Heavy Atom Count). [c]LLE: pIC_{50} − LogD. LogD measured via shake-flask method in octanol and water at pH 7.4.

https://doi.org/10.1021/acsmedchemlett.3c00453
ACS Med. Chem. Lett. 2024, 15, 1151−1158

yielding IC_{50} values in excellent agreement with the biophysical K_d values (Table 1).

In order to guide the further improvement of the pyrimidinone series, we wished to obtain structural data concerning MUS81-EME1-ligand interactions. We were able to obtain crystals of MUS81-EME1 in complex with DNA following previously reported procedures,[15,16] however, we were unable to observe electron density for any inhibitors when added either by soaking or cocrystallization. We next turned to hydrogen−deuterium exchange mass spectrometry (HDX-MS) as a means to obtain structural data concerning the site and mode by which the pyrimidinone compounds may be binding to the MUS81-EME1 complex. Comparison of HDX patterns following incubation of MUS81-EME1 with and without compound **10** showed clear protection of solvent-exposed backbone NHs surrounding the catalytic site of MUS81, strongly implying the compound binds to this site as anticipated, presumably via coordination with the Mg^{2+} ions expected to be present (Figure S2). This data gave us confidence in the binding site of compound **10** and compelled us to reassess our crystallographic system.

Inspection of the MUS81-EME1 crystal structures obtained by us, and others,[15,16] suggested that removal of the C-terminal "lobe" of the complex, which does not contain the catalytic site, may lead to a less dynamic protein complex and thereby aid crystallization. We therefore attempted to recombinantly express a protein construct composed of residues 246−462 of MUS81 and residues 246−455 of EME1 (referred to from hereon as "MUS81-EME1^N") in *E. coli.*[19] Soluble protein was

Table 2. Activity and Efficiency Metrics of Compounds 15, 18, 19, 20 against MUS81

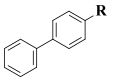

Cmpd	R	IC_{50} (μM)[a] SPR K_d (μM)[a]	LE[b] LLE[c]
15	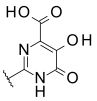	2.4 ± 0.2 0.72 (0.83)	0.33 5.9
18		0.66 ± 0.07 0.79 (0.72)	0.37 5.6
19	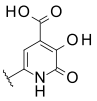	4.1 ± 0.6 1.4 (1.1)	0.32 6.5
20		1.1 ± 0.2 0.43 (0.88)	0.36 5.9

[a]IC_{50} and K_d values are the geometric mean ± SEM (for IC_{50} values) or geometric standard deviation (for K_d values) of at least three determinations. [b]LE (kcal/mol/HA): 1.37 × pIC_{50}/HAC (Heavy Atom Count). [c]LLE: pIC_{50} − LogD. LogD measured via shake-flask method in octanol and water at pH 7.4.

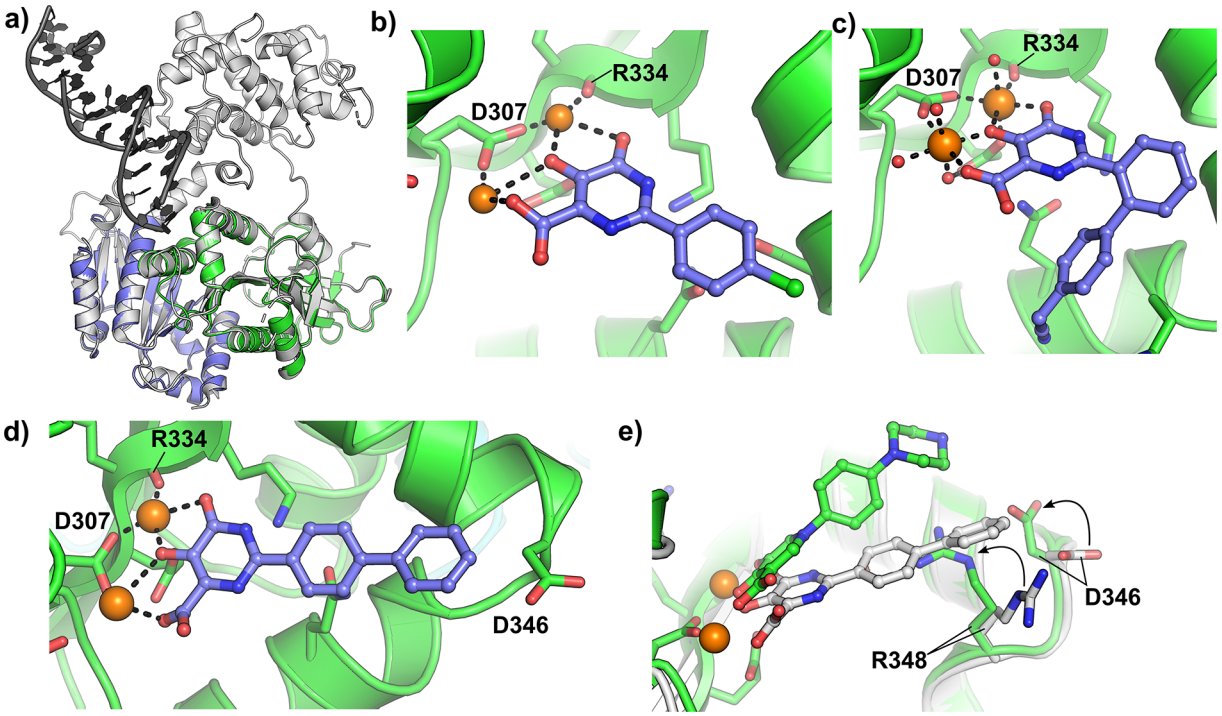

Figure 2. (a) Overlay of MUS81-EME1^N crystal structure reported here (MUS81, green; EME1, blue) with previously reported MUS81-EME1 crystal structure (PDB entry 4P0P, in light gray (protein) and dark gray (DNA)). RMSD of alignment = 0.940 Å for 327−327 C α atoms. (b−d) Crystal structures of MUS81-EME1^N bound by compounds **10**, **16**, and **15**, respectively. (e) Overlay of MUS81-EME1^N-**21** (green carbons) and MUS81-EME1^N-**15** (white carbons) complexes. Mg^{2+} ions are shown as orange spheres, polar contacts as black dashes. Crystallographic data collection and refinement statistics can be found in Table S1.

https://doi.org/10.1021/acsmedchemlett.3c00453
ACS Med. Chem. Lett. 2024, 15, 1151−1158

Table 3. Activity and Efficiency Metrics of Pyridinone Derivatives against MUS81

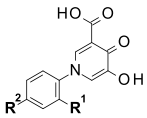

Cmpd	R^1	R^2	IC_{50} (μM)[a] SPR K_d (μM)[a]	LE[b] LLE[c]
18	H		0.66 ± 0.07 0.79 (0.72)	0.37 5.6
21	H		0.47 ± 0.08 2.0 (0.77)	0.38 7.1
22	CN		0.47 ± 0.12 1.2 (0.58)	0.35 6.7
23	H	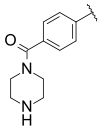	0.32 ± 0.04 0.67 (0.46)	0.29 6.9
24	CN	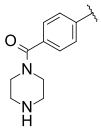	0.27 ± 0.04 1.1 (0.49)	0.27 7.6

[a]IC_{50} and K_d values are the geometric mean ± SEM (for IC_{50} values) or geometric standard deviation (for K_d values) of at least three determinations. [b]LE (kcal/mol/HA): 1.37 × pIC_{50}/HAC (Heavy Atom Count). [c]LLE: pIC_{50} − LogD. LogD measured via shake-flask method in octanol and water at pH 7.4.

Scheme 1. Synthesis of Amides 2−4[a]

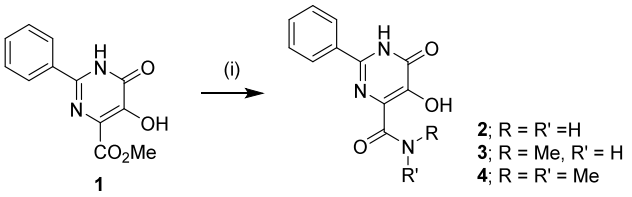

[a]Reagents and conditions: (i) RR'NH, MeOH, 80−140 °C.

readily obtained and purified, with *apo* crystallization experiments using commercially available protein crystallization screens yielding crystals in around 10% of the conditions tested. From these crystals, a 2.15 Å structure was obtained, revealing the truncated MUS81-EME1^N construct to adopt a conformation almost identical to that of the previous crystallization construct,[16] with an RMSD of 0.940 Å (Figure 2a). We next attempted to cocrystallize all compounds that had thus far given single-digit μM IC_{50} values (Table 1) with this truncated MUS81-EME1^N construct. These efforts yielded good quality electron density maps for MUS81-EME1^N crystals grown in the presence of compounds **10** and **12**. Structures determined for these compounds, although at modest resolutions (2.80 and 2.91 Å, respectively), showed both compounds to unambiguously bind to the catalytic site of MUS81, coordinating to two Mg^{2+} ions (themselves coordinated to residues D307, E333, and R334) of the protein) via the pyrimidinone moiety (Figures 2b and S3a). The naphthyl and chloro-phenyl groups occupy very similar positions, and are not buried within a pocket but sit in a shallow groove on the protein's surface (Figure S3a).

Following detailed inspection of these structures, two potential avenues for further improvement in the activity of the pyrimidinone series were evident: (1) the sterically unhindered (i.e., open) position of the phenyl group suggested significant scope for substitution of all positions of the ring, and (2) it appeared that interactions with the chelated Mg^{2+} ions were key to ligand binding, suggesting further optimization of the Mg^{2+}-binding (pyrimidinone) group to be potentially beneficial. To explore the phenyl ring of **5** further, we synthesized compounds with phenyl groups attached to the *ortho* (**13**), *meta* (**14**), and *para* (**15**) positions, with the *ortho*-substituted biphenyl further modified by the addition of a cyanomethyl group at the *para* position of the terminal phenyl group (**16**). While none of these modifications resulted in significantly increased affinity or biochemical activity, all were well-tolerated, giving single-digit μM K_d and IC_{50} values. We next attempted to cocrystallize these compounds (**13**−**16**) with MUS81-EME1^N. These experiments yielded two crystal structures: a 2.02 Å structure for **16** (Figure 2c) and a 2.73 Å structure for **15** (Figure 2d). The crystal structure of MUS81-EME1^N in complex with **16** shows the compound to clearly bind to the catalytic site via Mg^{2+} ion coordination (Figure 2c). Interestingly, the two crystallographically unique MUS81-EME1^N complexes of the asymmetric unit reveal **16** in two quite distinct orientations, 180 degrees relative to one another, while maintaining interactions with the Mg^{2+} ions (Figure S3b). This observation implied strongly that the interactions with the Mg^{2+} ions were driving the affinity between the compound and protein, and that the *ortho*-phenyl ring was contributing little to binding interactions.

The crystal structure of **15** again revealed the inhibitor to bind to the catalytic site of MUS81 via Mg^{2+} coordination (Figure 2d), with the compound overlaying very closely with that of the chloro-substituted (**10**) and naphthyl (**12**) compounds (Figure S3a). Interestingly, the terminal phenyl ring appeared to sit close to an acidic residue of MUS81 (D346), suggesting that a basic group at this position might increase affinity/activity (Figure 2d). Indeed, replacement of the terminal phenyl group of **15** with a piperazine group (**17**) led to an improvement, albeit modest (∼2-fold), in biochemical activity (Table 1).

Parallel to this work, we sought to further optimize inhibitor interactions with the catalytic Mg^{2+} ions. To achieve this, we synthesized and tested three pyridinone isomer analogues of the pyrimidinone **15** (**18**−**20**) (Table 2). Isomer **18** proved the most potent compound of the three, displaying an approximately 3-fold improvement in IC_{50} compared to the pyrimidinone equivalent (**15**).

With pyridinone **18** identified as our most potent Mg^{2+}-binding group, we combined this with the piperazinylphenyl moiety of the most potent pyrimidinone compound (**17**). This hybrid, **21**, resulted in a negligible increase in potency but a significant increase in LLE (from 5.6 (**18**) to 7.1 (**21**)) (Table 3). We next sought to optimize the pyridinone series further. Fortunately, we were able to obtain a cocrystal structure of **21** in complex with MUS81-EME1^N (refined to 2.36 Å), which, while indicating the compound to bind to the catalytic site by

https://doi.org/10.1021/acsmedchemlett.3c00453
ACS Med. Chem. Lett. 2024, 15, 1151−1158

Scheme 2. Synthesis of Hydroxy Pyrimidone Acids 7−17[a]

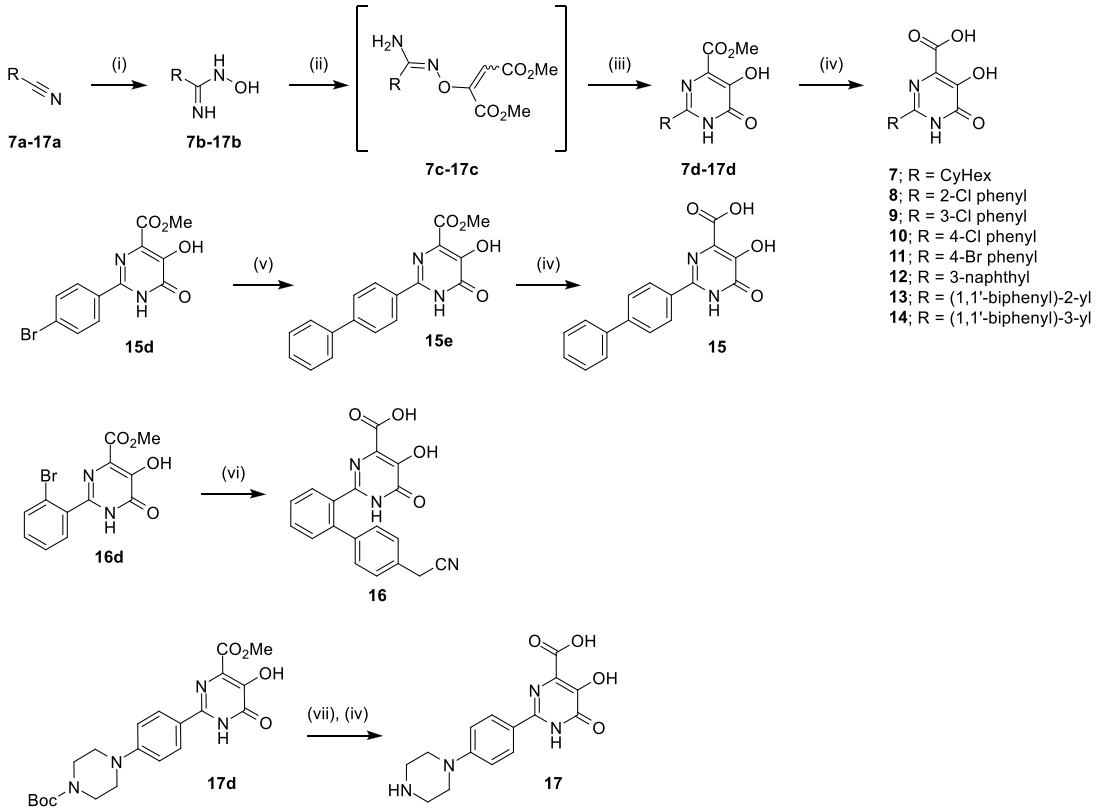

[a]Reagents and conditions: (i) 50% Hydroxylamine in water, EtOH, 70 °C; (ii) DMAD, $CHCl_3$, 60 °C; (iii) xylenes, 140 °C; (iv) LiOH, MeOH; (v) $PhB(OH)_2$, $Pd(dppf)_2Cl_2{\cdot}CH_2Cl_2$, Na_2CO_3, 1,4-dioxane/water, 100 °C; (vi) [4-(cyanomethyl)phenyl]boronic acid, RuPhos Pd G3, RuPhos, K_2CO_3, 1,4-dioxane/water, 120 °C; (vii) TFA, CH_2Cl_2, rt.

chelating to the two Mg^{2+} ions, also revealed some differences in the binding mode compared to the pyrimidinone series (Figure 2e). Specifically, the position of **21** appeared shifted relative to that of the pyrimidinones characterized structurally (e.g., **15**, see Figure 2e), with movement of the side-chain of R348 creating a new platform which the phenyl ring of **21**, which surprisingly is twisted by 90° relative to the pyridinone ring, packs onto. Unfortunately, the piperazine group did not appear to form any meaningful electrostatic contacts with the protein as hoped, however, the new orientation of the compound (relative to the pyrimidinone series, see Figure 2e), plus the twisted conformation of the phenyl ring, offered two further potential routes to optimize the pyridinone series. First, a nitrile group was attached to the *ortho* position of **21** (giving compound **22**) in an attempt to interact with (or displace) a crystallographic water molecule observed close to this position (Figure S3c). However, this modification did not result in any gain in potency for MUS81 (Table 3). Next, noting the position of D346 was still >4 Å from the piperazine group of **21**, we grew the compound further by inserting a benzoyl group in between the phenyl and piperazine groups (**23**), with an *ortho* nitrile substituted analogue (**24**) also synthesized. Both **23** and **24** displayed an approximately 2-fold improvement in biochemical activity against MUS81 (compared to **18**), with IC_{50} values of 0.32 and 0.27 μM, respectively (Table 3).

We next assessed the physicochemical and *in vitro* ADMET properties of top compounds **23** and **24** (Table S2). Both compounds display favorable physiochemical properties, with low logDs (<0) and high solubility (>200 μM), and excellent lipophilic ligand efficiencies (6.9 and 7.6 for **23** and **24**, respectively) (Tables 3 and S1). Compounds **23** and **24** were then assessed for metabolic stability in human liver microsomes (HLM) and rat hepatocytes (rHep), with both showing promising stability, with HLM and rHep Clint values of <3 μL/min/mg and 11 μL/min/1 × 10^6 cells and 7 μL/min/mg and 10 μL/min/1 × 10^6 cells for **23** and **24**, respectively (Table S2). The potential for efflux using the Caco2 assay was also assessed, with both **23** and **24** displaying low efflux ratios (1.5 and 1.1, respectively) (Table S2). **23** and **24** were also assessed for their ability to inhibit the hERG ion channel (*in vitro*), with both compounds giving IC_{50} values >40 μM. Both compounds were further screened against a safety panel (Eurofins SafetyScreen panel) of 22 common off-targets, comprising enzymes, receptors and ion channels (e.g., COX2, PDEs, INSR, GABA, NMDA, CaV-L). Pleasingly, neither compound showed any safety concern, with IC_{50} values >100 μM.

The main synthetic routes used to explore the SAR are shown in Schemes 1−4. Based on the original hit **1**, several amide analogues (**2**−**4**) were prepared via aminolysis of ester **1** (Scheme 1). Additionally, a number of close analogues to **1** were available commercially including acids **5** and **6**.

The series of hydroxy pyrimidone acids **7**−**17** were prepared following the method described by Culbertson[20] (Scheme 2). Commercial nitriles **7a**−**17a** were reacted with hydroxylamine to afford *N*-hydroxy amidines **7b**−**17b**, which were in turn treated with DMAD (dimethylacetylene dicarboxylate) to

https://doi.org/10.1021/acsmedchemlett.3c00453
ACS Med. Chem. Lett. 2024, 15, 1151−1158

Scheme 3. Synthesis of Hydroxy Pyrid-4-one Acids 18, 21−24[a]

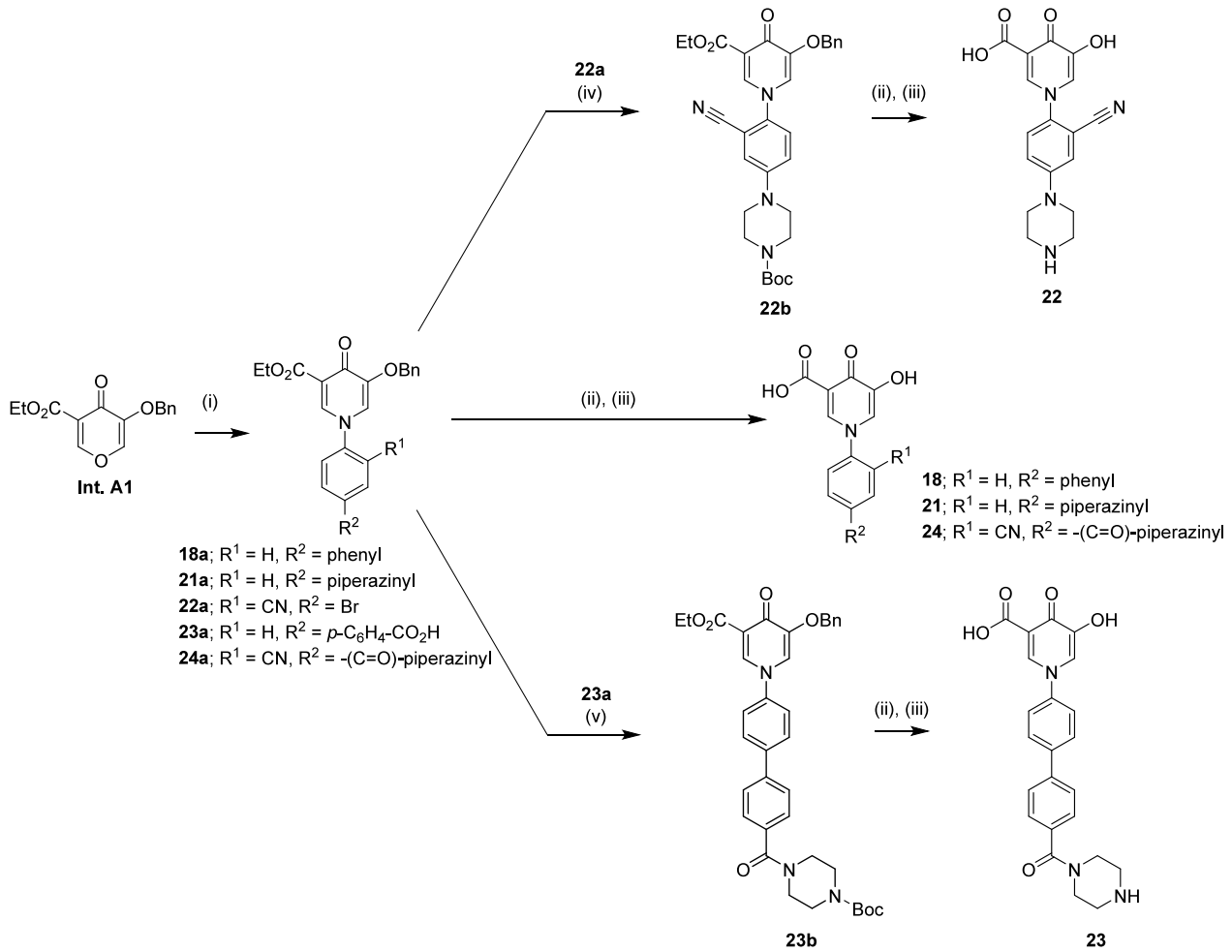

[a]Reagents and conditions: (i) Amine, AcOH, 50−90 °C; (ii) TFA, CH_2Cl_2, rt to reflux; (iii) LiOH, MeOH, rt to reflux; (iv) *tert*-butyl piperazine-1-carboxylate, $Pd_2(dba)_3.CHCl_3$, BINAP, Cs_2CO_3, 1,4-dioxane, 100 °C; (v) *tert*-butyl piperazine-1-carboxylate, HATU, DIPEA, DMF, rt.

Scheme 4. Synthesis of Regioisomeric Hydroxy Pyridone Acids 19 and 20[a]

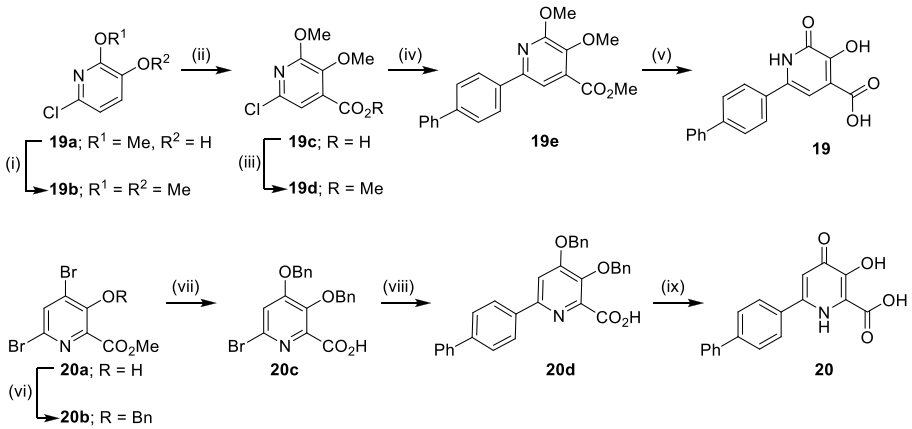

[a]Reagents and conditions: (i) NaH, MeI, THF, rt to 50 °C; (ii) *n*-BuLi, THF, −78 to 0 °C then CO_2, −78 °C to rt; (iii) $SOCl_2$, MeOH, reflux; (iv) [1,1′-biphenyl]-4-ylboronic acid, XPhos Pd G2, Cs_2CO_3, 1,4-dioxane/water, 100 °C; (v) BBr_3, CH_2Cl_2, rt then 30% HBr in AcOH, 120 °C; (vi) BnBr, Cs_2CO_3, DMF, rt; (vii) BnOH, NaH, DMF, 0 °C then 1 M NaOH; (viii) [1,1′-biphenyl]-4-ylboronic acid, $Pd(dppf)Cl_2{\cdot}CH_2Cl_2$, Na_2CO_3, DME/water, 80 °C; (ix) 10% Pd/C, H_2, THF/MeOH rt.

generate intermediates **7c−17c** via a Michael-type addition reaction. Intermediates **7c−17c** could be isolated but were often used directly without purification in the subsequent cyclization reaction to afford pyrimidone esters **7d−17d** which could then undergo base-mediated hydrolysis to hydroxy pyrimidone acids **7−14**. In addition, where the aromatic group

https://doi.org/10.1021/acsmedchemlett.3c00453
ACS Med. Chem. Lett. 2024, 15, 1151−1158

featured a halide (**15d** and **16d**) a Suzuki–Miyaura cross-coupling reaction could be employed to generate biphenyl derivatives. It was observed that under the aqueous conditions of the Suzuki reaction the ester was found to concomitantly hydrolyze to give the pyrimidone acid directly.

The synthesis of hydroxy pyrid-4-one acids **18**, **21**–**24** begins from pyrone **Int. A1** which was prepared as previously described in two steps from ethyl 4-(benzyloxy)-3-oxobutanoate.[21,22] Pyrone **Int. A1** reacted readily with a range of anilines in the presence of acetic acid which, following acidic debenzylation and ester saponification afforded compounds **18**, **21**, and **24** (Scheme 3). For **22** and **23**, it was first necessary to introduce the piperazine group by amide coupling or a Buchwald–Hartwig palladium catalyzed C–N cross-coupling reaction prior to global deprotection.

Few routes to highly substituted hydroxy pyridone acids have been previously described.[23] We were particularly interested in routes that would generate a protected hydroxy pyridone acid that would allow late-stage variation of the pendant aromatic group to aid SAR exploration (Scheme 4). To this end, 6-chloro 3-hydroxy pyridine **19a** was methylated and then the methoxy group was used to direct *ortho* lithiation and trapping with carbon dioxide to install the acid at C4. Following esterification, **19d** could then undergo a late-stage Suzuki cross-coupling reaction to install the biphenyl group prior to global demethylation using boron tribromide to afford **19**. In the case of **20**, it was convenient to start from dibromopyridine **20a** which was first protected as the benzyl ether **20b**. The key step was the selective S_NAr displacement of the C4-bromide which was achieved using the sodium alkoxide derived from benzyl alcohol. During this reaction some transesterification was observed so the mixture of methyl and benzyl esters were saponified directly to afford acid **20c**. A subsequent Suzuki cross-coupling reaction installed the biphenyl group which then afforded **20** following debenzylation.

We have reported here a fragment-based hit finding campaign targeting MUS81 from which we discovered novel inhibitors (**23** and **24**) with sub-μM biochemical activity and promising *in vitro* safety and ADMET properties. Crystal structures determined for several key compounds provide the first structural insight into MUS81 inhibition with small molecules and provide a basis for the further study of this potential cancer drug target.

■ ASSOCIATED CONTENT

Supporting Information

The Supporting Information is available free of charge at https://pubs.acs.org/doi/10.1021/acsmedchemlett.3c00453.

Full experimental details and additional figures and tables (PDF)

Accession Codes

All MUS81-EME1 crystal structures reported here have been deposited in the Protein Data Bank with the following accession codes: 9F98 (apo), 9F99 (**10**), 9F9A (**12**), 9F9K (**15**), 9F9L (**16**) and 9F9M (**21**).

■ AUTHOR INFORMATION

Corresponding Author

Gavin W. Collie – *R&D, AstraZeneca, Cambridge CB2 0AA, U.K.;* orcid.org/0000-0002-0406-922X; Email: gavin.collie@astrazeneca.com

Authors

Ulf Börjesson – *R&D, AstraZeneca, Gothenburg 431 83, Sweden*

Yunhua Chen – *Pharmaron Beijing Co., Ltd., Beijing 100176, P.R. China*

Zhiqiang Dong – *Pharmaron Beijing Co., Ltd., Beijing 100176, P.R. China*

Paolo Di Fruscia – *R&D, AstraZeneca, Cambridge CB2 0AA, U.K.*

Andrea Gohlke – *R&D, AstraZeneca, Cambridge CB2 0AA, U.K.*

Anna Hoyle – *R&D, AstraZeneca, Cambridge CB2 0AA, U.K.*

Thomas A. Hunt – *R&D, AstraZeneca, Cambridge CB2 0AA, U.K.;* orcid.org/0000-0003-1227-8862

Mehul H. Jesani – *R&D, AstraZeneca, Cambridge CB2 0AA, U.K.;* orcid.org/0000-0003-2070-3515

Haiou Luo – *Pharmaron Beijing Co., Ltd., Beijing 100176, P.R. China*

Jakub Luptak – *R&D, AstraZeneca, Cambridge CB2 0AA, U.K.;* Present Address: MRC Laboratory of Molecular Biology, Francis Crick Avenue, Cambridge, CB2 0QH, U.K

Alexander G. Milbradt – *R&D, AstraZeneca, Cambridge CB2 0AA, U.K.*

Priyanka Narasimhan – *R&D, AstraZeneca, Cambridge CB2 0AA, U.K.*

Martin Packer – *R&D, AstraZeneca, Cambridge CB2 0AA, U.K.*

Saleha Patel – *R&D, AstraZeneca, Cambridge CB2 0AA, U.K.*

Jingchuan Qiao – *Pharmaron Beijing Co., Ltd., Beijing 100176, P.R. China*

R. Ian Storer – *R&D, AstraZeneca, Cambridge CB2 0AA, U.K.*

Christopher J. Stubbs – *R&D, AstraZeneca, Cambridge CB2 0AA, U.K.*

Jonathan Tart – *R&D, AstraZeneca, Cambridge CB2 0AA, U.K.*

Caroline Truman – *R&D, AstraZeneca, Cambridge CB2 0AA, U.K.*

Anderson T. Wang – *R&D, AstraZeneca, Cambridge CB2 0AA, U.K.*

Matthew G. Wheeler – *R&D, AstraZeneca, Cambridge CB2 0AA, U.K.*

Jon Winter-Holt – *R&D, AstraZeneca, Cambridge CB2 0AA, U.K.;* orcid.org/0000-0002-7776-5963

Complete contact information is available at: https://pubs.acs.org/10.1021/acsmedchemlett.3c00453

Author Contributions

The manuscript was written through contributions of all authors. All authors have given approval to the final version of the manuscript.

Notes

The authors declare no competing financial interest.

■ ACKNOWLEDGMENTS

The following people are sincerely thanked for assistance with this work: Dr. Ross Overman, Dr. Benjamin Taylor, Wenzel Woltersdorf, Dr. William McCoull, and Dr. Jason Breed. We also thank the Soleil and DLS synchrotrons for providing access to data collection facilities and Dr. Peter McHugh and

Prof. Tom Brown (University of Oxford) for kindly contributing materials and expertise.

■ ABBREVIATIONS

CyHex, cyclohexyl; dppf, 1,1′-ferrocenediyl-bis-(diphenylphosphine); DSF, differential scanning fluorimetry; EME1, essential meiotic structure-specific endonuclease 1; HATU, 1-[bis(dimethylamino)methylene]-1*H*-1,2,3-triazolo-[4,5-*b*]pyridinium 3-oxid hexafluorophosphate; HDX-MS, hydrogen−deuterium exchange mass spectrometry; MUS81, methylmethanesulfonate and ultraviolet sensitive gene clone 81; RuPhos, 2-dicyclohexylphosphino-2′,6′-diisopropoxybiphenyl; SPR, surface plasmon resonance

■ REFERENCES

(1) Ciccia, A.; Constantinou, A.; West, S. C. Identification and characterization of the human mus81-eme1 endonuclease. *J. Biol. Chem.* **2003**, *278* (27), 25172−8.

(2) Ciccia, A.; McDonald, N.; West, S. C. Structural and functional relationships of the XPF/MUS81 family of proteins. *Annu. Rev. Biochem.* **2008**, *77*, 259−87.

(3) Matos, J.; West, S. C. Holliday junction resolution: regulation in space and time. *DNA Repair (Amst)* **2014**, *19* (100), 176−81.

(4) Wyatt, H. D.; Sarbajna, S.; Matos, J.; West, S. C. Coordinated actions of SLX1-SLX4 and MUS81-EME1 for Holliday junction resolution in human cells. *Mol. Cell* **2013**, *52* (2), 234−47.

(5) McPherson, J. P.; Lemmers, B.; Chahwan, R.; Pamidi, A.; Migon, E.; Matysiak-Zablocki, E.; Moynahan, M. E.; Essers, J.; Hanada, K.; Poonepalli, A.; Sanchez-Sweatman, O.; Khokha, R.; Kanaar, R.; Jasin, M.; Hande, M. P.; Hakem, R. Involvement of mammalian Mus81 in genome integrity and tumor suppression. *Science* **2004**, *304* (5678), 1822−6.

(6) Pamidi, A.; Cardoso, R.; Hakem, A.; Matysiak-Zablocki, E.; Poonepalli, A.; Tamblyn, L.; Perez-Ordonez, B.; Hande, M. P.; Sanchez, O.; Hakem, R. Functional interplay of p53 and Mus81 in DNA damage responses and cancer. *Cancer Res.* **2007**, *67* (18), 8527−35.

(7) Wu, F.; Liu, S. Y.; Tao, Y. M.; Ou, D. P.; Fang, F.; Yang, L. Y. Decreased expression of methyl methansulfonate and ultraviolet-sensitive gene clone 81 (Mus81) is correlated with a poor prognosis in patients with hepatocellular carcinoma. *Cancer* **2008**, *112* (9), 2002−10.

(8) Wu, F.; Shirahata, A.; Sakuraba, K.; Kitamura, Y.; Goto, T.; Saito, M.; Ishibashi, K.; Kigawa, G.; Nemoto, H.; Sanada, Y.; Hibi, K. Downregulation of Mus81 as a novel prognostic biomarker for patients with colorectal carcinoma. *Cancer Sci.* **2011**, *102* (2), 472−7.

(9) Xie, S.; Zheng, H.; Wen, X.; Sun, J.; Wang, Y.; Gao, X.; Guo, L.; Lu, R. MUS81 is associated with cell proliferation and cisplatin sensitivity in serous ovarian cancer. *Biochem. Biophys. Res. Commun.* **2016**, *476* (4), 493−500.

(10) Zeng, S.; Xiang, T.; Pandita, T. K.; Gonzalez-Suarez, I.; Gonzalo, S.; Harris, C. C.; Yang, Q. Telomere recombination requires the MUS81 endonuclease. *Nat. Cell Biol.* **2009**, *11* (5), 616−23.

(11) Lu, R.; Xie, S.; Wang, Y.; Zheng, H.; Zhang, H.; Deng, M.; Shi, W.; Zhong, A.; Chen, M.; Zhang, M.; Xu, X.; Shammas, M. A.; Guo, L. MUS81 Participates in the Progression of Serous Ovarian Cancer Associated With Dysfunctional DNA Repair System. *Front. Oncol.* **2019**, *9*, 1189.

(12) Zhong, A.; Zhang, H.; Xie, S.; Deng, M.; Zheng, H.; Wang, Y.; Chen, M.; Lu, R.; Guo, L. Inhibition of MUS81 improves the chemical sensitivity of olaparib by regulating MCM2 in epithelial ovarian cancer. *Oncol. Rep.* **2018**, *39* (4), 1747−1756.

(13) Zhong, A.; Zheng, H.; Zhang, H.; Sun, J.; Shen, J.; Deng, M.; Chen, M.; Lu, R.; Guo, L. MUS81 Inhibition Increases the Sensitivity to Therapy Effect in Epithelial Ovarian Cancer via Regulating CyclinB Pathway. *J. Cancer* **2019**, *10* (10), 2276−2287.

(14) Zhang, X.; Chen, X.; Lu, L.; Fang, Q.; Liu, C.; Lin, Z. Identification of small-molecule inhibitors of human MUS81-EME1/2 by FRET-based high-throughput screening. *Bioorg. Med. Chem.* **2023**, *90*, No. 117383.

(15) Chang, J. H.; Kim, J. J.; Choi, J. M.; Lee, J. H.; Cho, Y. Crystal structure of the Mus81-Eme1 complex. *Genes Dev.* **2008**, *22* (8), 1093−106.

(16) Gwon, G. H.; Jo, A.; Baek, K.; Jin, K. S.; Fu, Y.; Lee, J. B.; Kim, Y.; Cho, Y. Crystal structures of the structure-selective nuclease Mus81-Eme1 bound to flap DNA substrates. *EMBO J.* **2014**, *33* (9), 1061−72.

(17) The DSF screen was performed against recombinantly expressed and purified MUS81-EME1 hetereodimer with the following residue ranges: MUS81:246−551; EME1:246−570.

(18) Multiple parallel screening conditions were used in an attempt to enable the identification of magnesium chelating fragments from the primary screen. Fragments which induced a postive thermal shift only in the presence of 10 mM $MgCl_2$ were considered to be positive hits.

(19) Residue ranges for previously reported crystal structures of of human MUS81-EME1 (e.g., PDB entry 4P0P) are as follows: MUS81:246−551; EME1:178−570.

(20) Culbertson, T. P. Synthesis of methyl 5,6-dihydroxy-2-phenyl-4-pyrimidinecarboxylate: a corrected structure. *J. Heterocycl. Chem.* **1979**, *16*, 1423−1424.

(21) Kankanala, J.; Kirby, K. A.; Liu, F.; Miller, L.; Nagy, E.; Wilson, D. J.; Parniak, M. A.; Sarafianos, S. G.; Wang, Z. Design, Synthesis, and Biological Evaluations of Hydroxypyridonecarboxylic Acids as Inhibitors of HIV Reverse Transcriptase Associated RNase H. *J. Med. Chem.* **2016**, *59* (10), 5051−62.

(22) Kankanala, J.; Wang, Y.; Geraghty, R. J.; Wang, Z. Hydroxypyridonecarboxylic Acids as Inhibitors of Human Cytomegalovirus pUL89 Endonuclease. *ChemMedChem.* **2018**, *13* (16), 1658−1663.

(23) Credille, C. V.; Morrison, C. N.; Stokes, R. W.; Dick, B. L.; Feng, Y.; Sun, J.; Chen, Y.; Cohen, S. M. SAR Exploration of Tight-Binding Inhibitors of Influenza Virus PA Endonuclease. *J. Med. Chem.* **2019**, *62* (21), 9438−9449.

https://doi.org/10.1021/acsmedchemlett.3c00453
ACS Med. Chem. Lett. 2024, 15, 1151−1158